Corotating disk flow in an axisymmetric enclosure with and without a bluff body

Huey-Ming Tzeng
IBM Research Division, Almaden Research Center, San Jose, CA, USA

Joseph A. C. Humphrey
Department of Mechanical Engineering, University of California at Berkeley, Berkeley, CA, USA

An experimental study was performed for the airflow between a pair of coaxial disks corotating in an axisymmetric enclosure with and without an obstruction in the form of a rigid flat rectangular bluff body (arm). Long-term averages of the pressure coefficient across the arm and of the circumferential velocity component in the space between the disks were obtained as a function of position and disk angular velocity in a system of fixed dimensions. The unobstructed configuration exhibits an inner flow region approaching solid body rotation and an outer strongly sheared region with high turbulence levels. For this case, the assumption of steady axisymmetric flow allowed numerical calculations to be performed using the procedure of Chang et al. (1989). The calculations yield mean velocity distributions in good agreement with the unobstructed flow measurements but fail to reproduce some features of the velocity fluctuations that are believed to be due to circumferentially periodic mean flow structures. The measurements show that the presence of an arm has a profound effect on the flow.

Keywords: rotating disks; bluff body; turbulence; axisymmetric enclosure

Introduction

The fluid motion that arises in the space between a pair of corotating disks in a fixed enclosure is relevant to the turbomachinery industry and of special relevance to the computer industry since such a configuration is specific to magnetic-storage devices. Previous experimental research of this configuration in relation to disk drives has been primarily of a qualitative nature, consisting of flow visualization observations by Lennemann,[1] Picha and Eckert,[2] Kaneko et al.,[3] and Abrahamson et al.,[4] or limited to the hot-wire anemometry measurements of Picha and Eckert,[2] Kaneko et al.,[3] Tzeng and Fromm,[5] and Abrahamson et al.[4] More recently, the laser-Doppler anemometer (LDA) technique has been applied to investigate rotating disk systems with large[6] and intermediate[7] radius-to-disk spacing ratios.

We are concerned here with a stack of equidistant corotating disks in an axisymmetric enclosure where the fixed wall of the enclosure has a marked influence on the flow that arises in the space between any pair of disks. Figure 1 is a schematic (to scale except for dimension a) of a system composed of four disks. Numerical calculations of this type of configuration have been performed in the laminar[8] and in the turbulent[9] regimes. The work of Chang et al.[9] evaluated three turbulence modeling strategies and concluded that Prandtl's mixing length approach to simulate the turbulent viscosity, using a van Driest relation for the mixing length, was the best way to model the wall region in order to obtain accurate predictions of mean velocity. In that work, a two-equation (k-ε) turbulence model was used in the core of the flow. The evaluations in Chang et al.[9] were performed by comparing numerical predictions with the circumferential velocity measurements of Schuler et al.[7] The latter were obtained in a system, similar to that shown in Figure 1 with $H=9.53$ mm, $R_1/R_2=0.54$, $(R_2+a-R_1)/H=5.40$, and $a/H=0.28$ for disk speeds ranging between 50 and 4,000 rpm approximately.

The present work consists of an experimental investigation of the unobstructed axisymmetric configuration shown in Figure 1 with $H=4.0$ mm, $R_1/R_2=0.36$, $(R_2+a-R_1)/H=7.81$ and $a/H=0.25$ for 586, 1,171, 1,757, 3,513, and 5,269 rpm. The present configuration studied has a larger cross-section aspect ratio than that of Schuler et al.[7] and has been investigated over a different (lower) range of Reynolds numbers. The effect of obstructing the flow by introducing a bluff body (or "arm") of rectangular cross section midway between the disks has also been investigated. In the experiment, measurements of the time-averaged and root-mean-square (rms) circumferential velocity component were obtained with an LDA at various radial and axial locations. For the case of the arm inserted in the flow, time-averaged pressure measurements were also obtained. In addition, numerical calculations corresponding to the unobstructed experimental flow configuration were made using the turbulence model in Chang et al.,[9] described below.

The time-averaged measurements obtained in this investigation are of intrinsic fundamental value and provide a target for the development and testing of numerical calculation procedures purporting to predict strongly curved, highly three-dimensional, rotating turbulent shear flows. In this regard, the implications of assuming steady flow (in both the obstructed and unobstructed disk flow configurations) and circumferential symmetry (in the unobstructed case) are important issues for consideration and are discussed here.

Experimental apparatus and instrumentation

The experimental test section and its associated coordinate system are shown in Figure 1. Four rigid disks of outer radius

Address reprint requests to Dr. Humphrey at the Department of Mechanical Engineering, University of California at Berkeley, Berkeley, CA 94720, USA.

Received 23 October 1990; accepted 15 January 1991

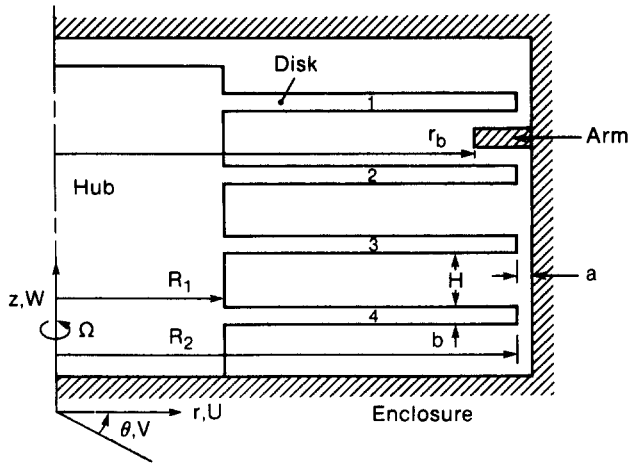

Figure 1 Corotating disk flow configuration with the coordinate system and velocity components defined. For the unobstructed flow case the arm was removed and the enclosure surface was smooth

$R_2 = 47.5$ mm were concentrically mounted on a hub. The topmost disk (1) was made of transparent polycarbonate material and was 1.4-mm thick. The other three disks were made of aluminum and were 1.25-mm thick. The disks were separated in the spindle axis direction (z direction) by three spacer rings of height $H = 4$ mm and radius $R_1 = 17.25$ mm. The disks were rotated by means of a spindle motor that was under closed-loop control such that long-term speed variations of less than 0.1 percent were achieved. The disk stack was surrounded by a cylindrical enclosure of inner radius $R_2 + a = 48.5$ mm. Three glass windows 2-mm thick and of inner curvature radius equal to 48.5 mm were installed at appropriate locations to facilitate the LDA velocity measurements. The test section was mounted on an x-y translation stage, which could be displaced horizontally relative to the fixed measurement point in either the radial or the axial direction of the test section.

The green (514.5 mm) light component of an argon-ion laser (Lexel Model 95) was used as the light source for the LDA, which was operated in the dual-beam backward scatter mode. The relevant optical system parameters are listed in Table 1. The LDA optical setup and the x-y translation stage supporting the test section were mounted on the same optical table to minimize optical alignment problems.

The selection of seed particles for laser-Doppler measurements represents a compromise between large particles (diameter > 10 μm), which are good light scatterers, and small particles (diameter < 1 μm), which follow the air flow very accurately. In this experiment it was found that a satisfactory compromise could be obtained by atomizing silicon oil (Aldrich Cat. no. 17563-3) in an aerosol generator (TSI Model 9306A at 20 psig). The mean diameter of these droplets was estimated to be 1 μm. In the course of an experimental run, silicon-oil droplets were blown several times into the test section. Care was taken to resume measurements of velocity only after the perturbations induced were of negligible magnitude. Once introduced into the test section, the droplets remained in suspension between the disks long enough to obtain reproducible time-averaged measurements at the locations of interest.

The band-pass filtered output signal of the photomultiplier tube (TSI Model 9160) was the input to a counter-type signal processor (Macrodyne Model 3000) to obtain the velocity information. The Doppler signal was validated by the 5/8 scheme to within six significant digits. The signal processor was interfaced with an IBM PC/XT operated in direct access mode, thus allowing the transfer of digitized data from the counter to the PC. At each location, 1,000 measurements were made of the circumferential velocity component from which the time-averaged and rms values were determined.

Flow conditions were investigated with and without an arm present in the space between the two disks examined; these were disks 1 and 2 counting from the top of the stack shown in Figure 1. The entire arm was 50 mm long and of rectangular cross section (5 × 1 mm). It could be inserted to different penetration depths along the symmetry plane between the two disks, through a snug-fitting slot in the enclosure wall. The longest dimension of the arm was aligned in the radial direction while maintaining its wider surfaces parallel to the disks. Velocity measurements were obtained with the arm extending 20 mm into the disk space, meaning that the tip of the arm was at $r_b = 28.5$ mm relative to the axis of rotation. As in the case of unobstructed flow, time-averaged measurements of the circumferential velocity component and its rms were obtained at specific circumferential locations upstream and downstream of the arm.

To facilitate the pressure measurements, a separate arm of identical geometry to the one above was fabricated. It had two 0.125-mm diameter pressure tap holes drilled on the upstream and downstream faces of the arm. They were located 1 mm from the arm tip and halfway along the thickness direction. Pressure gauges (Dwyer models 2000-6 and 2000-50) were employed for measuring the time-averaged pressure difference between the flow approaching and leaving the arm. Pressure measurements were taken with the tip of the arm successively located at $r_b = 28.5$, 33.5, and 38.5 mm.

Experimental uncertainties

Various sources of uncertainty contribute to the random and systematic errors in the mean and rms velocity measurements. These include index of refraction effects that alter the half-angle between the beams and the optical probe volume location; velocity bias, filter bias, and velocity gradient broadening; particle seeding and particle deposition considerations; finite size of the data samples; and disk wobble and variations in disk rotation speed.

The optical probe volume positioning uncertainty was kept to less than ±0.04 mm by the careful determination of an initial reference location and using stepping motors with incremental steps equal to 0.25 μm. The formulae for refraction corrections in Azzola and Humphrey[10] were used to verify that the 2-mm thick curved glass windows had a negligible effect on optical probe volume position and the beam half-angle. The rotation velocity of the disks spacer, at $r = R_1$, was measured to check the factor used for converting the Doppler frequency shift to units of velocity.

The nonuniform axial deposition of oil droplets on the glass windows contributed to the random uncertainty of all the velocity measurements as well as to the systematic uncertainty of these measurements made along axial traverses. By scattering

Table 1 Laser-Doppler anemometer optical parameters

Laser power	0.33 W
Laser wavelength	514.5 nm
Beam diameter at e^{-2}	1.3 mm
Beam half-angle	4.82°
Focal length	480 mm
Fringe spacing	3.1 μm
Number of fringes	48
Calculated dimensions of sample volume at e^{-2} (major and minor axes of ellipsoid)	1.7, 0.15 mm
Field stop aperture	0.13 mm
PMT pinhole diameter	15 μm

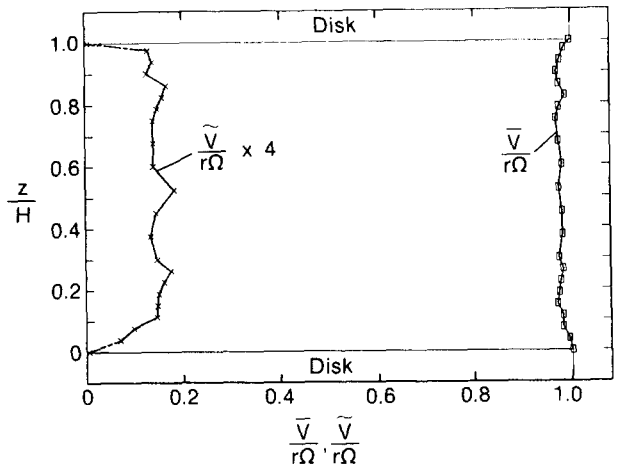

Figure 2 Axial distribution of the average and rms circumferential velocity components between two disks at $r=34.5$ mm ($r^*=0.57$). The disks rotate at 1,757 rpm

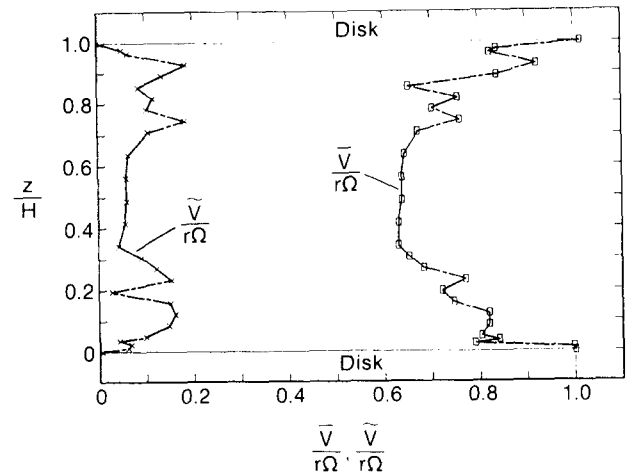

Figure 3 Axial distribution of the average and rms circumferential velocity components between two disks at $r=47.5$ mm ($r^*=1$). The disks rotate at 1,757 rpm

off the hub surface directly and comparing the hub velocity determined this way with the velocity determined from the output of the encoder in the closed loop control, it was possible to show that the component of random error was negligible, especially for the radial traverses made along the symmetry plane between the two disks. While it was not possible to determine the systematic component of uncertainty in the axial profiles, the differences in profile symmetry shown in Figures 2 and 3 give some idea of its magnitude.

Of the uncertainties specifically attributable to the LDA technique, filter bias, velocity bias, and gradient broadening were carefully examined. Filter bias was avoided by monitoring and adjusting the counter filter bandwidth. The maximum velocity bias was estimated to be less than 2 percent but, typically, it was about 0.5 percent. The effect of gradient broadening was most severe in a thin layer of fluid sheared by the curved enclosure wall so that most of the data was unaffected. In the flow region measured, typical uncertainties in the mean and rms velocities due to this effect were 1 to 2 percent and 1 to 5 percent, respectively. The small values of these errors over the bulk of the flow did not warrant correcting the data.

Following Dring[11] we have estimated that the small size of the silicone oil particles used($\simeq 1$ μm) guaranteed the tracking of velocity fluctuations higher than 45,000 Hz to better than 1 percent speed accuracy and with a phase lag of less than 8°. Similarly, particle drift velocity due to the centrifugal force can be shown to be negligibly small. Validated data rates ranging between 10 and 100 Hz were maintained in the course of an experimental run by periodically seeding particles in the flow.

Calculations of the mean and rms values of the circumferential velocity were made from samples consisting of 1,000 data points. The resulting statistical uncertainties were typically ± 2 percent for mean velocity and ± 4 percent for the rms.

The pressure measurements are the result of long-time averages obtained with one of two pressure gauges (Dwyer model 2000-6 and 2000-50) covering different ranges in the experiment. The resolutions of these two gauges are 1 and 2 mm of water, respectively, amounting to an uncertainty of less than ± 8 percent for the bulk of the pressure measurements.

In this study the amount of disk wobble was measured to be less than 20 μm peak to peak for all disks. Disk rotation was maintained constant to within ± 0.1 percent during the course of an experimental run. Both of these uncertainties had a negligible effect on the precision of the data.

Experimental results

The average, $\bar{V}$, and rms, $\tilde{V}$, circumferential velocities were measured along a radial line at the midplane ($z/H=0.5$) between disks 1 and 2 at five rotational speeds corresponding to 586, 1,171, 1,757, 3,513, and 5,269 rpm. They were selected to cover the rotational speed range of typical disk drives. The corresponding disk Reynolds numbers, $\mathrm{Re}\equiv\Omega R_2 H/\nu$, are 7.8×10^2, 1.6×10^3, 2.3×10^3, 4.7×10^3, and 7.0×10^3, respectively. In this definition of the disk Reynolds number, Ω is the angular velocity of the disks and ν is the kinematic viscosity of air.

Figure 4 shows the five measured velocity distributions, with velocity normalized by the local disk surface velocity $r\Omega$, where r is the local radius. Two flow regions, separated by a critical radius $r_c=34$ mm (corresponding to a value of the dimensionless radius $r^*\equiv(r-R_1)/(R_2-R_1)=0.55$) are observed. These consist of an inner region ($r<r_c$) where the air velocity is within 10 percent of the disk velocity and an outer region ($r>r_c$) where the normalized velocity decreases linearly to $\simeq 63$ percent of the disk velocity at the disk edge ($r=47.5$ mm, $r^*=1$). The velocity profiles show that, in general, the mean velocity increases in the inner region with increasing disk Reynolds number. This is attributed to the cross-stream secondary

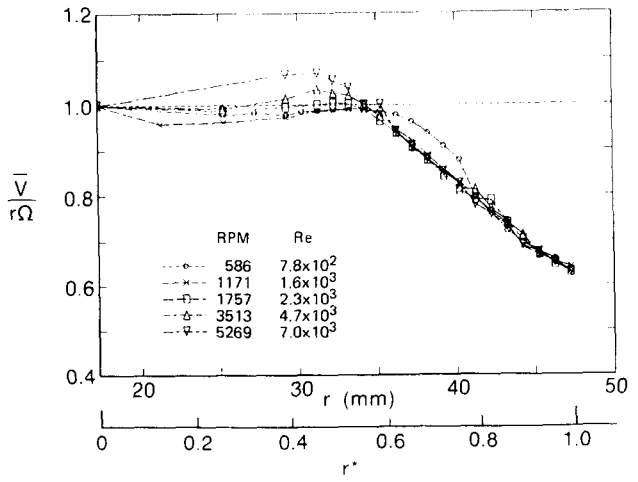

Figure 4 Radial distribution of the average circumferential velocity component midway between two disks for the conditions shown

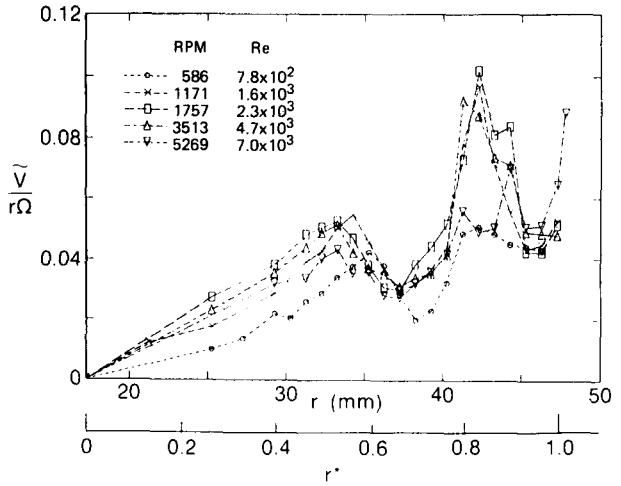

Figure 5 Radial distribution of the rms circumferential velocity component midway between two disks for the conditions shown

motion that displaces the maximum value of $\bar{V}$ toward smaller values of r with increasing Re and was confirmed by corresponding numerical calculations presented further below.

Except for the lowest Reynolds number case, the profiles in Figure 4 collapse to a single curve in the outer flow region. The scaling analysis performed by Schuler et al.[7] shows that this is the expected form of the circumferential velocity profile in the core of the flow (i.e., away from all fixed and moving surfaces) for large values of the Reynolds number.

The radial distributions of the rms velocity fluctuations are displayed in Figure 5. The overall trend is for the fluctuations to increase with the radius as the highly sheared region near the enclosure wall is approached. However, all the curves display intermediate maxima at about $r=33$ to 34 mm ($r^*=0.52$ to 0.55), which is very close to the location of r_c marking the transition between solid body rotation and sheared flow. Large values of the rms velocity have also been measured by Schuler et al.[7] in the inner and outer regions of a similar rotating disk flow configuration. Analysis of their velocity time histories reveals a nonturbulent sinusoidal component of motion. Visualization of the present flow configuration by Tzeng and Fromm,[12] using a strobed laser sheet to illuminate the suspended oil particles, and of related flow configurations by Lennemann[1] and Abrahamson et al.,[4] supports the notion that the sinusoidal motion is due to the periodic passage of circumferentially distributed foci with strong axial component of vorticity in this type of flow. These foci are responsible for large radially directed inflows and outflows of air, which account for the relatively high fluctuation levels around $r=r_c$ that cannot be attributed solely to the much smaller scale of turbulent motion.

Axial distributions of the average and rms circumferential velocity components at 1,757 rpm are plotted in Figures 2 and 3 for $r=34.5$ mm ($r^*=0.57$) and 47.5 mm ($r^*=1.0$), respectively. At $r=34.5$ mm the average and rms velocity distributions are fairly uniform, while at $r=47.5$ mm both distributions show strong variations with distance normal to the disks. These trends are in keeping with a solid body rotation-type flow in the inner region and a strongly sheared flow near the enclosure wall. Numerical calculations of this flow revealed a cross-stream secondary motion that drives fluid radially outward along the disk surfaces and radially inward midway between a pair of disks. This results in the convection of highly turbulent lower speed fluid into the core of the flow. The unusually large scatter shown by the data in Figure 3 for values of $0<z/H<0.3$ and $0.7<z/H<1.0$ is attributed to the nonuniform axial deposition of oil droplets along the enclosure wall in these ranges of z/H.

The insertion of an arm extending from the stationary enclosure wall to $r_b=28.5$ mm ($r_b^*=0.37$) strongly modifies the unobstructed flow field. Figure 6 displays the radial distribution of the average circumferential velocity component at 68°, 180°, and 292° downstream of the arm at a rotational speed corresponding to 3,513 rpm. The results are compared with the unobstructed flow case. At 68° downstream of the arm, blocking of the flow by the arm has induced an acceleration of the flow in the remaining space such that the average circumferential velocity is higher than the local disk velocity at $r=24.5$ mm ($r^*=0.24$). The magnitude of the average circumferential velocity component in the wake of the arm (28.5 mm $<r<$ 47.5 mm) changes very little (less than 8 percent) between the 68° and 292° downstream stations. The radial distribution of the rms fluctuations, plotted in Figure 7, shows large fluctuation levels immediately downstream of the arm that fall below the unobstructed flow case at 180° and 292°. The disappearance at $r=r_c$ of the large fluctuations observed for unobstructed flow is due to the shearing by the arm of the circumferentially

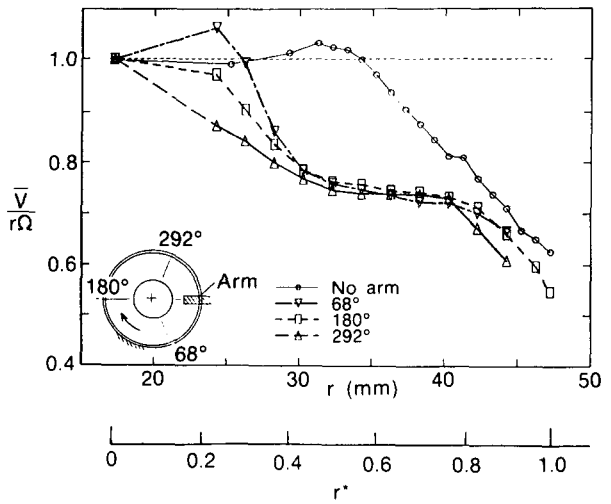

Figure 6 Radial distribution of the average circumferential velocity component midway between two disks rotating at 3,513 rpm at three angular locations and in the presence of a rectangular arm penetrating up to $r_b=28.5$ mm ($r^*=0.37$)

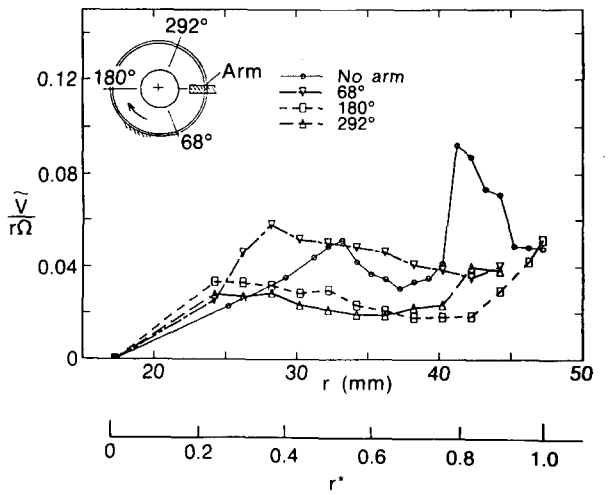

Figure 7 Radial distribution of the rms circumferential velocity component midway between two disks rotating at 3,513 rpm at three angular locations and in the presence of a rectangular arm penetrating up to $r_b=28.5$ mm ($r^*=0.37$)

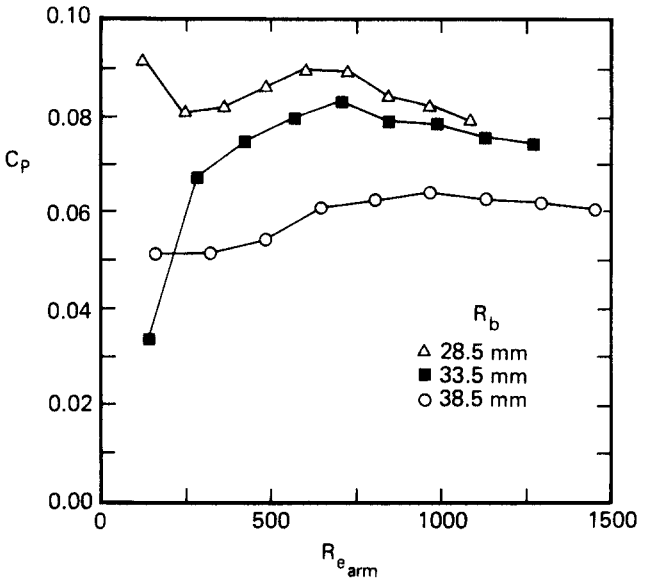

Figure 8 Pressure coefficient for flow past a rectangular arm midway between two disks for three penetration depths

distributed vortical structures that contribute to the rms. The rms data suggest that these structures are not reestablished within one rotation cycle.

The pressure coefficient, C_p, is plotted against the arm Reynolds number, Re_{arm}, in Figure 8 for three arm penetration depths corresponding to $r_b = 28.5$, 33.5, and 3.85 mm, or, $r_b^* = 0.37$, 0.54, and 0.70, respectively. The definition for C_p is $\Delta p/(\frac{1}{2}\rho r^2\Omega^2)$ where Δp is the time-averaged pressure difference measured across the arm in the flow direction and r in this case is the disk radius corresponding to the center of the pressure tap hole. The arm Reynolds number is defined as $Re_{arm} \equiv r_b \Omega t/\nu$ where t is the arm thickness normal to the flow direction. The disk rotational speed was varied as in the cases of velocity measurements. The data show that the pressure coefficient increases with arm penetration depth and that, for fixed penetration, it increases and subsequently levels off with increasing Re_{arm}.

Numerical calculations

Calculations were performed for the unobstructed disk flow configuration. The numerical procedure and turbulence model employed are extensively discussed by Chang et al.[9] A summary of relevant information is provided here followed by a discussion of the results obtained for the present flow configuration.

The use of wall functions to impose boundary conditions on velocity in the complex corotating disk flows of interest here is not successful because the forms of the required functions are simply not known in sufficient detail. Low-Reynolds number model formulations that account for wall-damping effects on the velocity fluctuations represent attractive alternatives because they do not employ wall functions. However, they are computationally intensive and not yet thoroughly researched.[13] A less rigorous but much simpler way to resolve the wall layer flow is to use the van Driest relation, within the context of a Prandtl mixing length model, to specify the mixing length near walls. Such an approach has been used successfully to calculate swirling turbulent boundary layers over rotating disks, cones, and cylinders by Koosilin et al.,[14] and in rotating cavities by Chew,[15,16] and Chew and Vaughan.[17]

The work of Chang et al.[9] shows that the assumption of steady, circumferentially symmetric flow in the space between a pair of corotating disks leads to good predictions of mean velocity and heat transfer when using the van Driest relation for the mixing length. A modification of this relation, which accounts for strong variations of the shear stress and curvature near walls, further improved their predictions of mean velocity but yielded poorer results for the distribution of turbulent kinetic energy in the flow.

In this work we have applied the model of Chang et al.[9] which employs an unmodified van Driest relation for the flow near walls (rotating or fixed) and a standard two-equation k-ε model in the core of the flow. The relevant transport equations describing the flow are given in that reference. In the model, a generalized form of the Boussinesq assumption is employed to relate the turbulent shear stress to the mean rate of strain via an isotropic turbulent viscosity, ν_t. In the core of the flow this is calculated from the turbulent kinetic energy, k, and its rate of dissipation, ε, according to $\nu_t = C_\mu k^2/\varepsilon$ where $C_\mu = 0.09$ is a model constant. In the wall region ν_t is obtained from the generalized form of Prandtl's mixing length hypothesis wherein $\nu_t = l_0^2 P_k^{1/2}$ with

$$P_k = 2\left[\left(\frac{\partial \bar{U}}{\partial r}\right)^2 + \left(\frac{\partial \bar{W}}{\partial z}\right)^2 + \left(\frac{\bar{U}}{r}\right)^2\right] + \left[\frac{\partial \bar{W}}{\partial r} + \frac{\partial \bar{U}}{\partial z}\right]^2 + \left[r\frac{\partial}{\partial r}\left(\frac{\bar{V}}{r}\right)\right]^2 + \left[\frac{\partial \bar{V}}{\partial z}\right]^2$$

and the mixing length, l_0, specified from the van Driest relation

$$l_0 = \kappa y\left[1 - \exp\left(-\frac{y^+}{26}\right)\right]$$

In this equation, κ is the von Karman constant, y is the distance from the wall, and y^+ is the wall coordinate given by $y^+ = y u_\tau/\nu$ where $u_\tau = (\tau_w/\rho)^{1/2}$ is the wall friction velocity.

At the interface between the wall region and the core flow, the two submodels are matched by requiring that the turbulent viscosity vary continuously and assuming that the turbulence is in equilibrium. These two requirements provide the necessary boundary conditions for calculating k and ε in the core of the flow. The conditions are that: $k = l_0^2 P_k/C_\mu^{1/2}$ and $\varepsilon = l_0^2 P_k^{3/2}$. By trial and error, the matching interface is fixed to lie between $y^+ = 10$ and 50.

The solution of the continuity and momentum equations requires a specification of boundary conditions. For this the disks were assumed to be negligibly thin and to be contained in an infinite disk stack. (This configuration corresponds to case 1 investigated by Chang et al.[9]) With reference to Figure 1, the flow was assumed to be symmetrical with respect to the horizontal plane between any two disks at $z/H = 0.5$. At this plane the axial ($\bar{W}$) velocity component and the axial (z) gradients of $\bar{U}$, $\bar{V}$, k, and ε were set equal to zero. The no-slip condition was imposed on all solid surfaces for $\bar{U}$, $\bar{V}$, and $\bar{W}$. Because of the matching condition described above, boundary conditions for k and ε are not required at solid surfaces. A symmetry plane boundary condition was imposed for all variables in the gap region between the tip of the disk and the enclosure wall.

The calculation domain was subdivided into a variable density calculation grid, with control volumes (or cells) geometrically defined at the grid nodes for scalar quantities, and between grid nodes for the velocity components. Finite difference approximations to the conservation equations were derived by volume integration about each cell, subject to specific rules concerning the evaluation of fluxes and source terms described by Patankar.[18] Global second order accuracy of the difference equations was achieved by using Leonard's[19] QUICK scheme (as improved by Freitas et al.[20]) for convective transport terms, and central differencing for the diffusion terms.

The set of algebraic finite difference equations was solved recursively using the tridiagonal matrix algorithm. This was done within the context of the REBUFFS (LeQuere et al.[21]) solution procedure, which is iterative in nature. In the calculation sequence, initial values for all the dependent variables of the flow field are guessed or specified from a previous calculation. The cross-stream velocity components are then solved and a pressure correction is evaluated using the SIMPLE procedure of Patankar.[18] The pressure correction is used to update the pressure and cross-stream velocity components, respectively, and, from these quantities, the circumferential velocity component is obtained. At this point, the k and ε equations are solved using near wall values for k and ε evaluated from the matching condition discussed above. The iteration sequence is repeated until the convergence criterion is satisfied; this is that the largest of the normalized residuals for mass or momentum be less than 5×10^{-5}.

The numerical procedure has been carefully tested in the laminar flow regime.[8] Additional tests for turbulent flow were conducted with reference to several of the rotating disk flow configurations investigated in Schuler et al.,[7] Bakke et al.,[22] and Northrop and Owen.[23,24] The results of the tests, reported by Chang et al.,[9] served four purposes: (1) they established the nature of the grids required to generate grid-independent results; (2) they allowed an evaluation of the assumption of steady axisymmetric flow, on which the numerical approach is based; (3) they facilitated a relative ranking of the three turbulence models investigated; and (4) to within the accuracies of the measurements and the turbulence model approximations, they confirmed that rotation, heat transfer, and blowing effects were correctly predicted. The comparisons performed were favorable, showing that the van Driest/Prandtl mixing length model is capable of accurate predictions of mean velocity and heat transfer and qualitatively correct distributions of turbulent kinetic energy.

Based on the successive grid refinement checks conducted by Chang et al.,[9] the calculations performed for this study were obtained on a nonuniform grid with $z = 26 \times r = 62$ nodes. It is estimated that further grid refinement would have led to changes of less than 2 percent in the results predicted for rotational speeds less than 4,000 rpm, approximately. The calculations were carried out on the Berkeley Campus Cray X-MP computer and typically required 360 cpu seconds to achieve convergence in about 2,000 iterations.

Plots of predicted cross-stream and circumferential components of motion for 3,513 rpm are shown in Figure 9. This condition corresponds to one of the cases investigated experimentally. The plots serve to convey an impression of the flow, showing the cross-stream recirculation cells that arise near the enclosure wall and their attendant effect on the circumferential component of motion. The calculations show that between $r^* = 0$ and 0.6 the bulk of the flow between the disks approaches solid-body rotation. Between $r^* = 0.8$ and 1.03, the imbalance

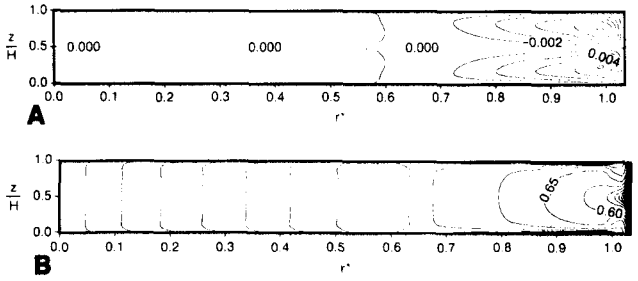

Figure 9 Contour plots of predicted streamlines (A) and mean circumferential velocity (B) in the cross-stream plane for 3,513 rpm

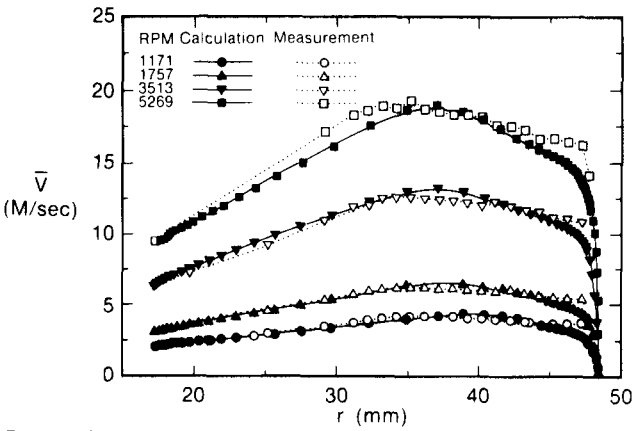

Figure 10 Comparison between measurements and predictions of the average circumferential velocity component midway between two corotating disks without an arm

between the inwardly directed radial pressure gradient and the outwardly directed centrifugal force sets up the cross-stream flow observed. The secondary motion leads to penetration of fluid with low circumferential velocity and high turbulent kinetic energy from the enclosure wall into the core along the assumed symmetry plane. Direct numerical simulations by Tzeng and Fromm[12] for the present configuration, assuming axisymmetric but unsteady flow conditions, suggest that the cross-steam flow stagnation point on the curved enclosure wall is unstable, causing the secondary cells to oscillate in size and intensity.

Figures 10 and 11 provide a comparison between measurements and calculations of the mean and rms values of the circumferential velocity component for the present study. The measurements and computations of mean velocity results are in good agreement for the three lowest rpm, except near the enclosure wall where the model appears to underpredict the velocity. This discrepancy may be partly due to the above-referenced cross-stream flow oscillation, which are not modeled numerically. At the highest rpm, 5,269, the calculations also underpredict the mean circumferential velocity in the solid body rotation region of the flow. At this high rpm, it is critical to resolve the very thin boundary layers flowing along the disk surfaces in order to predict the mean cross-stream secondary flow accurately. Because the calculation grid was optimized for 4,000 rpm or less, it is possible that the resolution required at higher rpm was impaired. Underprediction of the secondary flow along the disks surfaces would lead to a weaker displacement of the circumferential velocity component in the direction of the inner wall, as observed.

Calculations of the corresponding rms velocity are in broad qualitative agreement with the measurements. In Figure 11 measurements of $\tilde{V}$ are compared with calculations of $(\frac{2}{3}k)^{1/2}$. If the predictions were partly adjusted for the anisotropy that is known to exist among the normal stresses,[25] by multiplying by a factor equal to 1.3, better agreement would be obtained. Notwithstanding, the calculations fail to reproduce the maximum in $\tilde{V}$, which is observed between $r = 30$ and 40 mm. As explained above, this peak is associated with axially aligned, large-scale coherent flow structures that are distributed (more or less periodically) in the circumferential direction. The structures induce large deviations from the mean velocity and, therefore, contribute significantly to the measured rms. However, the assumption of steady axisymmetric motion precludes the numerical prediction of their contribution to the rms. It is likely that circumferential and cross-stream flow unsteadiness in the experiment also contribute to the differences observed between measurements and calculations of V nearer the enclosure wall.

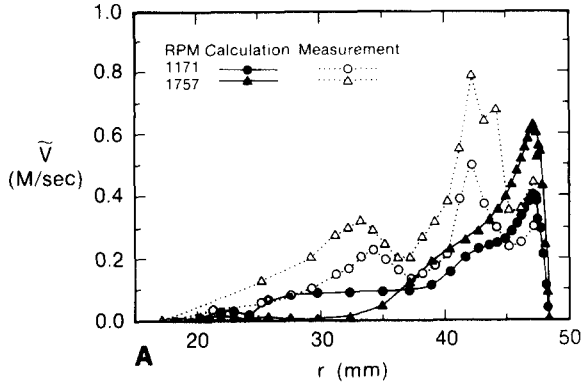

Figure 11A Comparison between measurements and predictions of the rms circumferential velocity component midway between two corotating disks without an arm for the condition shown

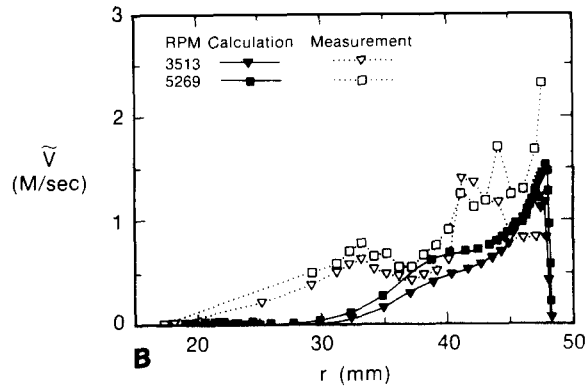

Figure 11B Comparison between measurements and predictions of the rms circumferential velocity component midway between two corotating disks without an arm for the condition shown

Further work, involving experimental and numerical time-resolution of the flow, as performed in Schuler et al.[7] and Tzeng and Fromm,[12] respectively, is necessary to satisfactorily resolve these points.

Summary and conclusions

Time-averaged measurements of the circumferential velocity component and its rms were obtained in the space between a pair of disks rotating in an axisymmetric enclosure. Obstructed and unobstructed conditions were examined and numerical calculations of the latter case were performed. In the unobstructed case, the configuration geometry was fixed and the effects of varying disk speed of rotation were examined. With the obstruction present, the disk speed was fixed and the effect of arm obstruction was investigated. The following are the main conclusions of this study.

(1) There exists a critical radius, r_c, that separates the flow between a pair of corotating disks into two regions. One, the inner region, approaches the condition of solid body rotation. The other, the outer region, is strongly sheared and highly turbulent. In this work, $r_c^* \simeq 0.55$ over the range $7.8 \times 10^2 \leq \mathrm{Re} \leq 7.0 \times 10^3$.

(2) At the interface between the inner and outer flow regions, the rms of the circumferential velocity attains an intermediate maximum value. This is attributed to the presence of axially aligned, organized (meaning nonturbulent) circumferentially period structures that contribute to the oscillatory component of motion.

(3) Due to the strong secondary cross-stream flow that arises in the space between a pair of disks corotating in an axisymmetric enclosure, the circumferential velocity along the symmetry plane between the disks can exceed the local disk velocity. The extent of the region influenced by this effect increases with increasing disk rotation speed.

(4) The presence of a radially aligned obstruction, in the form of an arm of rectangular cross-section, substantially alters the flow field in the space between a pair of corotating disks. Measurements of velocity show that the flow is temporarily accelerated past the arm in the region of flow left unobstructed, between the tip of the arm and the hub. Further downstream, however, the bulk of the flow in the region obstructed by the arm is decelerated to values of velocity considerably less than those corresponding to the unobstructed flow case. It would appear that most of the arm remains in its own wake as the flow completes a cycle. In the present case of large obstruction (arm extended from shroud to $r_b < r_c$) the maximum in the rms velocity observed at r_c^* in the unobstructed flow does not appear in the obstructed flow case. We conclude that shearing by the arm destroys the coherence of the axially aligned structures responsible for this maximum. Measurements of the arm pressure coefficient show that this quantity increases with increasing obstruction penetration and that it tends to a constant value (for a given penetration) with increasing rpm.

(5) Numerical calculations were performed for the experimental flow conditions of this study. A high Reynolds number model of turbulence was used in the core of the flow. This was matched to a mixing length formulation in the near wall region. The calculations show good agreement with the measured mean circumferential component of velocity and qualitative agreement with the corresponding rms. The discrepancies observed for the rms are partly due to the isotropic nature of the model. However, the assumption of steady, axisymmetric flow, precludes resolving the large-scale, oscillatory components of motion known to exist in the flow and that contribute to the rms fluctuation.

Future work should include measuring velocity time histories and their associated spectra in both obstructed and unobstructed corotating disk flow configurations. In this regard, special attention should be paid to understanding the interactions that arise between the length and time scales associated with disk rotation and those imposed by the presence of an obstruction, such as the arm investigated in this work. This information is relevant to rendering predictable the behavior of configurations where significant fluid-system component interactions are expected to arise.

Acknowledgments

The authors are pleased to acknowledge valuable discussions held with J. E. Fromm during the course of this work. Thanks are due to C. J. Chang for help in performing the numerical calculations. We are especially grateful to L. Harlow for his invaluable assistance in fabricating the pressure-sensing arm used in the obstructed flow configuration. We are indebted to B. Schechtman and T. O'Sullivan for their support of this project. The study was conducted while the second author was a visiting research scholar at the IBM Almaden Research Center. An earlier version of this paper was reported at the 7th Symposium on Turbulent Shear Flows, Stanford, August 1989.

References

1 Lennemann, E. Aerodynamic aspects of disk files. *IBM Journal of Research and Development*, 1974, **18**, 480

2 Picha, K. G., and Eckert, E. R. G. Study of the air flow between coaxial disks rotating with arbitrary velocities in an open or enclosed space. *Proc. 3rd. U.S. National Congress on Applied Mechanics*, 1958, 791

3 Kaneko, R., Oguchi, S., and Hoshiya, K. Hydrodynamic characteristics in disk packs for magnetic storage. *Review of the Electrical Communications Laboratories*, 1977, **25**, 1325

4 Abrahamson, S. D., Koga, D., and Eaton, J. E. The flow between shrouded corotating disks. *Phys. Fluids A*, 1989, **1**, 241

5 Tzeng, H.-M., and Fromm, J. E. Study of airflow between a pair of corotating, centrally-clamped disks in a stationary, cylindrical enclosure. Paper presented at the *Fortieth Annual Meeting of the American Physical Society, Division of Fluid Dynamics*, November 22–24, 1987

6 Szeri, A. Z., Schneider, S. J., Labbe, F., and Kaufman, H. N. Flow between rotating disks. Part 1. Basic flow. *J. Fluid Mech.*, 1983, **134**, 103

7 Schuler, C. A., Usry, W. B., Weber, B., Humphrey, J. A. C., and Greif, R. On the flow in the unobstructed space between shrouded corotating disks. *Phys. Fluids A*, 1990, **2**, 1760

8 Chang, C. J., Schuler, C. A., Humphrey, J. A. C., and Greif, R. Flow and heat transfer in the space between two corotating disks in an axisymmetric enclosure. *J. Heat Transfer*, 1989, **111**, 625

9 Chang, C. J., Humphrey, J. A. C., and Greif, R. Calculation of turbulent convection between corotating disks in axisymmetric enclosures. *Int. J. Heat and Mass Transfer*, 1990, **33**, 2701

10 Azzola, J., and Humphrey, J. A. C. Developing turbulent flow in a 180° curved pipe and its downstream tangent. LBL Report No. 17681, University of California at Berkeley, 1984

11 Dring, R. P. Sizing criteria for laser anemometry particles. *J. Fluid Eng.*, 1982, **104**, 15

12 Tzeng, H.-M., and Fromm, J. E. Airflow study in a cylindrical enclosure containing multiple corotating disks. *Proc. 3rd Int. Symposium on Transport Phenomena and Dynamics of Rotating Machinery*, Honolulu, Hawaii, 1990

13 Patel, V. C., Rodi, W., and Scheuerer, G. Turbulence models for near-wall and low Reynolds number flows. A review. *AIAA J.*, 1985, **23**, 1308

14 Koosilin, M. L., Launder, B. E., and Sharma, B. I. Prediction of momentum, heat, and mass transfer in swirling, turbulent boundary layers. *J. Heat Transfer*, 1974, **96**, 204

15 Chew, J. W. Prediction of flow in a rotating cavity with radial outflow using a mixing length turbulence model. *Proc. 4th International Conference on Numerical Methods in Laminar and Turbulent Flow*, Swansea, UK, 1985

16 Chew, J. W. Computation of flow and heat transfer in rotating disc systems. *Proc. 2nd ASME-JSME Thermal Engineering Conference*, Hawaii, 1987, 361

17 Chew, J. W., and Vaughan, C. M. Numerical predictions for the flow induced by an enclosed rotating disk. *Proc. 3rd ASME International Gas Turbine Conference*, Amsterdam, 1988

18 Patankar, S. V. *Numerical Heat Transfer and Fluid Flow*, Hemisphere, McGraw-Hill, New York, 1980

19 Leonard, B. P. A stable and accurate convective modelling procedure based on quadratic upstream interpolation. *Comp. Method Appl. Mech. Engrg.*, 1979, **19**, 59

20 Freitas, C. J., Street, R. L., Findikakis, A. N., and Koseff, J. R. Numerical simulation of three-dimensional flow in a cavity. *Int. J. Numer. Methods Fluids*, 1985, **5**, 561

21 LeQuere, P., Humphrey, J. A. C., and Sherman, F. S. Numerical calculation of thermally driven two-dimensional unsteady laminar flow in cavities of rectangular cross section. *Num. Heat Transfer*, 1981, **4**, 249

22 Bakke, E., Kreider, J. F., and Kreith, F. Turbulent source flow between parallel stationary and co-rotating disks. *J. Fluid Mech.*, 1973, **58**, 209

23 Northrop, A., and Owen, J. M. Heat transfer measurements in rotating disc system. Part 1: The free disc. *Int. J. Heat and Fluid Flow*, 1988, **9**, 19

24 Northrop, A., and Owen, J. M. Heat transfer measurements in rotating disc systems. Part 2: The rotating cavity with a radial outflow of cooling air. *Int. J. Heat and Fluid Flow*, 1988, **9**, 27

25 Tennekes, H., and Lumley, J. L. *A First Course in Turbulence*. The MIT Press, Cambridge, Massachusetts, 1972